#111

FERMILAB-CONF-74-145-E A. Greene

Session A1

The Reaction $\pi^- p \to \pi^0 n$ Between 20 GeV/c and 100 GeV/c

A. V. Barnes, D. J. Mellema, A. V. Tollestrup, R. L. Walker
Department of Physics, California Institute of Technology, Pasadena

and

O. L. Dahl, R. A. Johnson, R. W. Kenney, M. Pripstein
Lawrence Berkeley Laboratory, University of California

ABSTRACT

Preliminary $d\sigma/dt$ distributions are presented for the pion charge exchange reaction $\pi^- p \to \pi^0 n$ ($0 < -t < 1.4$ $(\mathrm{GeV}/c)^2$). Incident π^- momenta were 20.7, 40.6, 66 and 101 GeV/c, obtained at the NAL Meson Laboratory. The effective Regge ρ trajectory for these data is discussed. The relationship between the new forward differential cross sections and existing data on $\pi^- p$ and $\pi^+ p$ total cross sections is examined.

AEC Contracts Nos. W-7405-eng-48 (LBL) and AT(11-1)-68 (CIT)

I. Introduction

An experiment is in progress at NAL to measure various neutral final state reactions of π^- mesons on protons. Preliminary results for the reaction:

$$\pi^- p \rightarrow \pi^o n \tag{1}$$

in the momentum interval 20 GeV/c to 100 GeV/c are reported here. In an accompanying paper [1] we give results for the reaction $\pi^- p \rightarrow \eta n$, and we report some evidence for production of other neutral final states, including $\eta' n$ and $\omega^o n$.

Pion nucleon charge exchange is considered to be one of the simplest examples of the Regge mechanism because this reaction is dominated by the exchange of a single Regge trajectory, namely the ρ. However, polarization measurements [2] show that the interaction is more complicated than the exchange of a single trajectory. In order to investigate the Regge character of this reaction it is important to obtain measurements at high energy over as large an energy and momentum transfer range as possible. We have therefore measured the differential cross section $d\sigma/dt$ throughout the momentum transfer range from $-t=0$ to $-t \simeq 1.4$ $(\mathrm{GeV/c})^2$ at momenta from 20 to 100 GeV/c and have determined an effective ρ trajectory from these data in conjunction with published data from 5.9 to 18.2 GeV/c. [3]

Isospin invariance and the optical theorem imply a well-known relation between forward charge exchange scattering and the difference, $\Delta\sigma$, between the total cross sections for $\pi^- p$ and $\pi^+ p$ scattering, as given by the following expression:

$$\left.\frac{d\sigma_{CEX}}{dt}\right|_{t=0} = \frac{\pi}{p_{lab}^2} (1 + R^2) (\mathrm{Im}\, A_{CEX}(0))^2 = 25.5 (1 + R^2) (\Delta\sigma)^2. \tag{2}$$

where R is the ratio of real to imaginary parts of the forward charge exchange

scattering amplitude, p_{lab} is the laboratory beam momentum in units of GeV/c, $d\sigma/dt$ is in $\frac{\mu b}{(GeV/c)^2}$ and $\Delta\sigma$ is in mb. In Section IV we make use of a result from field theory to estimate R from our measured ρ trajectory. On the basis of this information we use equation (2) to predict $\Delta\sigma$ as a funtion of p_{lab}. These predictions are then compared with existing data on $\sigma_T(\pi^{\pm}p)$.

II. Description of Experiment

Identifying the individual reactions under study and distinguishing them from background are of crucial importance. The charge exchange cross section at 101 GeV/c is approximately 10^{-4} times the π^-p total cross section and about 1/10 the cross section for producing final states consisting solely of neutral particles. The serious background comes from reactions such as $\pi^-p \rightarrow \pi^0N^*$, where the π^0 is indistinguishable from a valid charge exchange π^0. Detection of low energy photons from the N^* decay ($N^* \rightarrow n\pi^0$, $\pi^0 \rightarrow \gamma\gamma$) identifies this reaction as background.

The experimental arrangement is shown schematically in Figs. 1 and 2. The apparatus is designed to measure those neutral final state reactions in which all photons are within the acceptance of the γ-ray detector. The reaction kinematics are then determined solely from the photon measurements.

An incident π^- in the beam is tagged by a threshold Cerenkov counter, and the pion position and angle are measured by counter hodoscopes H1 and H2. The beam geometry is defined by counters M1, M2, M3 and A0, where halo particles are rejected by A0. The double cell liquid hydrogen target is 60 cm long and is surrounded by scintillation counters A1, A2 and A3 which are used to inhibit an event trigger whenever charged particles are produced in the final state. In addition there are shower veto counters which do not

participate in the trigger logic but rather tag the presence of final state photons outside the acceptance of the γ-ray detector. The shower veto counters upstream and downstream of the target are multi-layer lead scintillator shower detectors, having five lead plates totaling either 5 or 10 radiation lengths. The shower veto counters closely surrounding the hydrogen target (the "veto house") are of similar construction, except that they consist of plastic Cerenkov detector instead of scintillator in order to minimize their sensitivity to recoil neutrons from charge exchange events. There are eight lead plates in every veto house counter; four plates are each one-quarter of a radiation length in thickness and four are one radiation length each. This arrangement with two thicknesses of lead plates ensures a high detection efficiency for low energy photons, even for those incident at highly oblique angles. The photon veto system covers the entire 4π solid angle except for the detector solid angle and the 5 cm x 5 cm beam entrance hole.

The π^0 detector is a hodoscope detector which measures the x and y (transverse coordinates) distributions of the energy deposited in one or more photon showers, integrated over the axial (incident beam direction) coordinate z. The detector is shown schematically in Fig. 3. It is constructed of 19 lead plates, each 6.4 mm thick and 75 cm square. The plates are stacked normal to the direction of incident particles (z) with gaps between them of approximately 7 mm. These gaps are filled with long narrow scintillation fingers, 1.05 cm wide, which are close-packed and run the full width of the detector. Vertical and horizontal fingers are in successive gaps. The eight fingers having the same x coordinate or the same y coordinate are connected optically by curved light pipes at one end, and each set of eight fingers so connected constitutes one counter. There are 70 x-counters and 70 y-counters. Each finger has been separately wrapped with foil of

graded reflectivity, and a light trap captures those rays transmitted at large angles to the finger axis. Because of this special treatment, each counter yields pulses of uniform height (within 2%) over the entire counter length.

By simultaneously measuring all pulse heights, h_{xi} and h_{yi} $(1 \leq i \leq 70)$, in the detector counters it is possible to find the energy E, mass M, and production angle of a particle decaying at the target into the photons observed by the detector. The first three spatial moments of the pulse height distribution are given by

$$E_x = \sum_i h_{xi} \quad ; \quad E_y = \sum_i h_{yi}$$

$$\bar{x} = \frac{1}{E_x} \sum_i x_i h_{xi} \quad ; \quad \bar{y} = \frac{1}{E_y} \sum_i y_i h_{yi}$$

$$\overline{x^2} = \frac{1}{E_x} \sum_i x_i^2 h_{xi} \quad ; \quad \overline{y^2} = \frac{1}{E_y} \sum_i y_i^2 h_{yi}$$

E and M^2 are then evaluated from the spatial moments using the following expressions:

$$E = \frac{1}{2} (E_x + E_y)$$

$$\left(\frac{M}{E}\right)^2 = \frac{1}{L^2} \left[(\overline{x^2} - \bar{x}^2) + (\overline{y^2} - \bar{y}^2) - 2\,\delta^2 \right]$$

where L is the distance from the target to the detector and δ^2 is a constant which is an approximate measure of the inherent width of a single shower of half the total energy. The coordinates $(\bar{x}, \bar{y})$ are a good estimator of the point of intersection between the detector and the extrapolated trajectory of the decaying particle. The production angle is then computed from $(\bar{x}, \bar{y})$ and the π^- beam hodoscope information. These relations are based on the small angle approximation and hold for particles decaying in any decay orientation

and into any number of photons as long as all of the photons enter the detector.

The trigger logic requires the following:

1. The incident pion must be within the acceptance of the beam-defining counters.
2. There must be no incident charged particle accompanying the trigger pion within a time interval of ± 50 ns, including the halo region.
3. The incident π^- must interact in the target and there must be no charged particles in the final state.
4. Within the critical parts of the anticoincidence system there must be complete recovery from any large pulses arising from a previous interaction.
5. The on-line computer must be ready to accept a new event.

When a successful trigger occurs, a complete set of data on that event is read into the computer and written on magnetic tape for subsequent analysis. A sample of the events is analyzed on-line in order to display plots of current operating conditions and up-to-date results. Tag bits are recorded for the hodoscope counters, the Cerenkov counter and all of the photon shower anticoincidence counters. Pulse heights are recorded for the 140 photon detector counters, for the Cerenkov counter, for the charged particle veto system (A_2 and A_3) and for each of the shower anticounters. The pulse height analyzer system contains 180 channels of 2200 bins each. Input pulse heights are digitized in parallel within 100 microseconds. The output information is read serially at a rate limited by the computer, taking up to 2 ms for the complete readout of an event. These kinds of data, with our loose trigger conditions, permit a flexible off-line treatment of each event and allow subsequent analysis of the effects of each cut parameter.

III. Selection of Events

The trigger condition assured that a final state was completely neutral. The cut structure listed in the following table comprises the off-line selection criteria used in selecting the sample of charge exchange events.

1. The CLEAN requirement. There must be no pulse in any photon veto counter, thereby eliminating events with photons outside the solid angle of the detector.
2. Cerenkov Tag. A pulse in the threshold Cerenkov counter is required, thereby eliminating kaons and antiprotons from the beam flux.
3. Energy in the π^0 detector. The measured energy was required to be within the full energy peak corresponding to the incident π^- beam energy.
4. Number of photons. It was required that two individual showers be resolved by the detector for the charge exchange reaction.
5. Cosθ cut. In the decay $\pi^0 \rightarrow \gamma\gamma$, the emission angle θ of the photons in the π^0 rest frame with respect to the π^0 line-of-flight can be calculated from the data. Those events having emission angles with $|\cos\theta| > 0.7$ are eliminated because one photon has very small laboratory energy near $\cos\theta = 1.0$. This arbitrary cut is well outside the region where the detection efficiency falls below 100%.
6. Mass cut. The value of the mass M measured by the detector is required to be within the π^0 mass peak.

The distribution in M^2 for events satisfying criteria 1-5 (mass cut not imposed) is shown in Fig. 4. The level of the background outside the π^0 mass peak is very low, permitting clean identification of π^0 events. Moreover, the mass spectra for the one photon and three photon events (not shown) exhibit no peak in the π^0 region, indicating very little

loss of events from the two photon category.

In calculating cross sections it is necessary to correct for the loss of genuine reaction (1) events which are eliminated from our data sample by various cuts, and to correct for the inclusion of background events in the data sample. These corrections are listed in Table I. Most of the corrections were measured directly from the data or from several special runs interspersed with the data collection. Several of these corrections are for well-defined physical processes for which a reliable calculation can also be made; wherever possible the empirically determined corrections were verified by calculation.

The fraction of recoil neutrons detected by the veto house was empirically measured by examining the pulse height distribution as a function of the azimuthal angle of the π^0 and thus, of the recoil neutron. A similar analysis was carried out for the charged veto counters on a sample of data collected for this purpose. The efficiencies of the veto house counters as a function of energy for both photons and neutrons were also measured using a tagged photon beam at the Stanford Mark III accelerator and a tagged neutron beam at the LBL 184" cyclotron.

As an additional check on our overall normalization we measured the $\pi^- p$ total cross section at 40 GeV/c using the same beam logic and liquid hydrogen target. Our result of $\sigma = (24 \pm 2)$ mb is in good agreement with the 50 GeV/c result of 24.1 mb reported by Baker et al. [11]

IV. Results:

The preliminary distributions of $d\sigma/dt$ for reaction (1) at 20.7, 40.6, 66 and 101 GeV/c are given in Fig. 5. At 20.7 GeV/c the region of good acceptance for π^0's was confined to a limited range of momentum transfer,

and thus we present data for this energy only between $-t = 0$ and 0.5 $(GeV/c)^2$. For the three higher energies the data is presented over the range $0 < -t < 1.4$ $(GeV/c)^2$. In Fig. 6 we show the small t region, with horizontal error bars at the bottom of this figure indicating typical values of the experimental t resolution (Δt) at 101 GeV/c. The total number of events at each energy for reaction (1) is listed in Table II. The data show a characteristic forward peak with a small dip at t=0 and a break around $-t \approx 0.6$ $(GeV)c)^2$. These features are similar to those observed at lower energies [3, 4, 5, 6, 7], although the dip at t=0 is more pronounced in our data than in the highest energy data (48 GeV/c) of Bolotov et al. [4], where it is essentially absent. The presence of a forward dip in the data from 20 to 100 GeV/c suggests that the strong spin-flip contribution which is evident at energies below 20 GeV/c persists at high energies. The position of the break near $-t=0.6$ $(GeV/c)^2$ shows no obvious systematic variation with energy over the range from 40 GeV/c to 100 GeV/c and appears to be consistent with the position of the dip observed in data for reaction (1) down to an incident momentum of 3 GeV/c [3].

A value for $(d\sigma/dt)_{t=0}$ at each energy has been extrapolated by fitting the data in the region $-t < 0.08$ $(GeV/c)^2$ to a second - order polynominal. The results are shown in Table II.* Also in Table II are listed values for

$$\sigma_{CEX} = \int_{-1.5}^{0} \frac{d\sigma}{dt}\, dt \qquad (3)$$

at each energy. These values are plotted in Fig. 7 as a function of incident beam momentum, along with integrated cross sections from other experiments [3-7].

*The πN amplitude analysis at 6 GeV/c [15] indicates a very steep t dependence for the non-flip amplitude of reaction (1) near t = 0. In this case, our polynomial extrapolation to t = 0 could be systematically low by roughly 10%. A detailed study of this effect is in progress.

The data points from the present experiment appear to be systematically below those of Bolotov, et al. [4]. We have fitted the measured values of σ_{CEX} to a function of the form

$$\sigma_{CEX} = A p_{lab}^{-N}$$

using the data of this experiment along with the data of Ref. [3], spanning a range from 5.9 to 100 GeV/c incident momentum. The result of this fit is shown by the dashed curve in Fig. 7, with A = (679 ± 47) μb and N = 1.15 ± .07. Bolotov et al. [4] report values of A = (680 ± 50) μb and N = 1.12 ± 0.03 using their data and that of Ref. [3].

A study has been made of the effective Regge ρ trajectory by fitting data from reaction (1) to the functional form

$$\frac{d\sigma}{dt} = \frac{B}{sq^2} s^{2\alpha} \tag{4}$$

where α and B are parameters to be determined as a function of t, and q is the momentum of each particle in the CM system. An overall fit (Fit 1) from 6 to 100 GeV/c has been carried out at a number of t values, using the data of Ref. [3] and of the present experiment. The results of this fit are summarized in Table III, and plots of dσ/dt versus p_{lab} are given in Fig. 8 for several representative values of t. The curves in Fig. 8 show the best fit to (4) at each of these t values. The fitted values of α are displayed in Fig. 9(a). By way of comparison, we also show in Fig. 9(a) the values of α obtained by fitting the data of Refs. [3] and [4] from 6 to 50 GeV/c (Fit 2), as reported in Ref. [4]. We have not attempted a fit including both our data and the data of Ref. [4] because of the inconsistency between their results and our preliminary results.

There is reasonable agreement between these two sets of α's in the range $0.05 < -t < 0.6$ $(GeV/c)^2$. However, at small t the values of α from Fit 1 appear to flatten out and approach an intercept value $\alpha(0) \simeq 0.50$, whereas the values of α from Fit 2 are more linear in the small t region and approach an intercept value $\alpha(0) \simeq 0.58$. For $-t > 0.6$ $(GeV/c)^2$, there is an indication that the effective trajectory from Fit 1 lies somewhat above the trajectory obtained in Fig. 2.

To investigate further the behavior of Fit 1 in the small t region, we have fit separately the data of Ref. [3] from 6-18 GeV/c (Fit 3) and the data of the present experiment from 20-100 GeV/c (Fit 4). (In Fit 4 we have determined values of α only for $-t < 0.5$ $(GeV/c)^2$, since the 20.7 GeV/c data is restricted to this t-region. Without the 20.7 GeV/c data, the s-interval of the remaining data is too small to obtain a meaningful fit.) The results of Fits 3 and 4 are listed in Table III and are plotted in Fig. 9(b).

For $-t < 0.2$ $(GeV/c)^2$ Fit 3 lies systematically above Fit. 4. The non-linearity of Fit 1 at small t is not obvious in either Fit 3 or Fit 4 and may be an artifact of combining two sets of data with different energy dependence into the same fit. A possible interpretation of the systematic difference between Fit 3 and Fit 4 is that equation (4) does not adequately describe the energy dependence of reaction (1) over the entire range from 6 to 100 GeV/c. This point may be clarified when new data at energies above 100 GeV/c become available from the present experiment.

Invoking the general principles of axiomatic field theory and assuming a power law dependence on s for the forward charge exchange amplitude, one can obtain [10] the ratio R of the real to the imaginary part of the forward

charge exchange amplitude:

$$R = \tan \frac{\pi\alpha(o)}{2} \tag{5}$$

This ratio is independent of s, given the validity of the power law assumption of equation (4).

Over the range from 20 to 100 GeV/c we adopt a value of $\alpha(o) = 0.50$ based on Fit 4, and from expression (5) we would then obtain R = 1.00. However, if the power law assumption is not rigorously correct, as is possibly suggested by the effective trajectory analysis, then R would differ from this value and would vary as a function of s. In the present case, we estimate from a dispersion calculation that R would be greater than 1 (typically 1.08) between 20 and 100 GeV/c, taking the difference between Fit 3 and Fit 4 at face value.

We have computed two predictions for $\Delta\sigma = \sigma_T(\pi^- p) - \sigma_T(\pi^+ p)$ from 20 to 100 GeV/c, using expression (2) with R = 1.08. One prediction, shown by the solid curve in Fig. 10, uses the values of $(d\sigma/dt)_{t=0}$ given in Table II. As discussed above, the polynomial extrapolation to t = 0 may lead to a value which is systematically low by about 10%. Therefore, we have computed a second prediction, in which the values of $(d\sigma/dt)_{t=0}$ in Table II have been increased by 10%. This second calculation is shown by the dashed curve in Fig. 10.

Neither curve is entirely in agreement with the trend of existing data from $\pi^- p$ and $\pi^+ p$ total cross section measurements [11-14]. The solid curve is low throughout the entire energy range. Although the dashed curve is consistent with the NAL data of Ref. [11] at 50 and 100 GeV/c, it apparently would be too low if extended to 150 and 200 GeV/c. Both predictions fall

systematically below the Serpukhov total cross section data of Ref. [12]. At 20 GeV/c the dashed curve is in good agreement with the BNL data of Ref. [13], but the predicted energy dependence is too steep to describe total cross section data below 20 GeV/c.

V. Acknowledgments

The authors wish to acknowledge those who have made contributions to various phases of this experiment:

J. F. Bartlett for important sections of computer software, particularly for the on-line analysis system;

M. A. Wahlig for his important contributions dating from the earliest phases of the experiment, particularly in the veto system design and testing;

D. Eartley for his work on the Cerenkov counter and for on-site logistics and scheduling; the personnel of the Fermi National Accelerator Laboratory, especially P. Koehler, R. Lundy, and H. Haggerty of the Meson Laboratory, for their complete cooperation and assistance in bringing the experiment into operation;

G. C. Fox and R. D. Field for helpful discussions on the theory and phenomenology of charge exchange reactions.

References

1. O. L. Dahl et al., "The Reaction $\pi^- p \to \eta n$ Between 20 GeV/c and 100 GeV/c", submitted to XVII International Conference on High Energy Physics, 1974.
2. D. Hill et al., Phys. Rev. Lett. 30, 239 (1973); P. Bonamy et al., Nucl. Phys. B52, 392 (1973); P. Bonamy et al., Nucl Phys. B16, 335 (1970); P. Bonamy et al., Phys. Lett. 23, 501 (1966); D Drobnis et al., Phys. Rev. Lett. 20, 274 (1968).
3. A. V. Stirling et al., Phys. Rev. Lett. 14, 763 (1965); P. Sonderegger et. al., Phys. Lett. 20, 75 (1966).
4. V. N. Bolotov et al., "Negative Pion Charge Exchange Scattering on Protons in the Momentum Range 20-50 GeV/c", Serpukhov Preprint, 1973; V. N. Bolotov et al., Phys. Lett. 38B, 120 (1972).
5. I. Mannelli et al., Phys. Rev. Lett. 14, 408 (1965); M. A. Wahlig and I. Mannelli, Phys. Rev. 168, 1515 (1968).
6. M. A. Azimov et al., JETP Lett. 3, 216 (1966).
7. V. V. Barmin et al., JETP 19, 102 (1964).
8. R. K. Logan, Phys. Rev. Lett. 14, 414 (1965).
9. G. Hoehler et al., Phys. Lett. 20, 79 (1966).
10. R. J. Eden, High Energy Collisions of Elementary Particles, Cambridge University Press, 1967, pp. 194, 212.
11. W. F. Baker et al., "Total Cross Sections of $\pi^{\pm}$, $K^{\pm}$, p and $\bar{p}$ on Hydrogen and Deuterium Between 50 and 200 GeV/c", Preprint, 1974.
12. S. P. Denisov et al., Nucl. Phys. B65, 1 (1973).
13. K. J. Foley et al., Phys. Rev. Lett. 19, 330 (1967).
14. A. Citron et al., Phys. Rev. 144, 1101 (1966).
15. G. C. Fox and C. Quigg, Ann. Rev. Nucl. Sci. 23, 219 (1973).

Table I

Cross Section Corrections for $\pi^- p \to \pi^0 n$

	20.7 GeV/c	40.6 GeV/c	66 GeV/c	101 GeV/c
Length of LH_2 target	40.1 cm	40.1 cm	40.1 cm	60.4 cm
Spurious charged veto				
γ-rays from π^-	-5%	-5%	-5%	-7%
Conversion of γ-rays	-5%	-5%	-5%	-6%
Recoil nuetron veto*	-2%	-2%	-2%	-2%
Accidentals	-5%	-2%	-4%	-6%
Spurious shower veto				
Recoil neutron veto*	-5%	-5%	-5%	-5%
Accidentals	-1%	-1%	-1%	-3%
π^0 detection efficiency				
Geomtrical acceptance*	-0.2%	0	0	0
$N_\gamma = 2$ cut	-0.5%	-0.5%	-0.5%	-0.5%
Cosine θ cut	-29%	-29%	-29%	-29%
$\pi^0 \to \gamma e^+ e^-$ Decay	-1%	-1%	-1%	-1%
Background				
Target empty	+3%	+4%	+4%	+3%
N^* contamination	+3%	+3%	+3%	+3%

*Averaged over t.

Table II

Preliminary Results for $\pi^- p \rightarrow \pi^0 n$

	Number of Events	$\frac{d\sigma}{dt}^*_{t=0}$	σ_{CEX}
20.7 GeV/c	3557	$(96 \pm 10)\mu b/(GeV/c)^2$	$(21.5 \pm 1.3)\mu b$
40.6	28804	(47 ± 3)	(9.4 ± 0.6)
66	11528	(28 ± 2)	(5.5 ± 0.3)
101	26995	(19 ± 2)	(3.3 ± 0.3)

*Obtained from polynomial extrapolation to t = 0. See footnote, page 8 for discussion of possible systematic error in extrapolation.

Table III

Effective Regge Trajectory Values
for $\pi^- p \rightarrow \pi^0 n$

	Fit 1	Fit 3	Fit 4
Range of p_{lab}	6-100 GeV/c	6-18 GeV/c	20-100 GeV/c
Data Used	Ref. 3 and Present Expt. (Prelim. Results)	Ref. 3	Present Expt. (Prelim. Results)
Values of α:			
$-t = 0.01$ $(GeV/c)^2$	0.493 ± 0.013	0.62 ± 0.05	0.48 ± 0.03
0.03	0.494 ± 0.014	0.56 ± 0.05	0.48 ± 0.02
0.05	0.499 ± 0.014	0.60 ± 0.05	0.46 ± 0.02
0.07	0.478 ± 0.014	0.52 ± 0.05	0.45 ± 0.02
0.09	0.461 ± 0.015	0.51 ± 0.06	0.45 ± 0.04
0.12	0.440 ± 0.014	0.47 ± 0.05	0.39 ± 0.04
0.16	0.412 ± 0.015	0.40 ± 0.05	0.36 ± 0.04
0.21	0.371 ± 0.015	0.40 ± 0.05	0.35 ± 0.04
0.28	0.316 ± 0.016	0.36 ± 0.06	0.34 ± 0.04
0.36	0.27 ± 0.02	0.28 ± 0.06	0.23 ± 0.05
0.45	0.15 ± 0.03	0.17 ± 0.08	0.18 ± 0.07
0.55	0.00 ± 0.05	-0.06 ± 0.14	
0.65	-0.04 ± 0.05	-0.11 ± 0.14	
0.80	-0.18 ± 0.04	-0.18 ± 0.14	
1.00	-0.31 ± 0.04	-0.14 ± 0.13	
1.20	-0.49 ± 0.07	-0.56 ± 0.18	

Figure Captions

Fig. 1 Schematic drawing of the experimental layout. The apparatus is designed to measure those neutral final state reactions in which all photons are within the acceptance of the γ-ray detector. V-1, V-2, V-3, V-4 and the Veto House comprise the shower veto system. A-2 and A-4 are part of the charged particle veto system.

Fig. 2 Detailed drawing of the experimental apparatus surrounding the liquid hydrogen target. H_1 and H_2 are counter hodoscopes which measure the incident π^- position and angle. A threshold Cerenkov counter (not shown) between H_1 and A_o tags pions in the beam. The beam geometry is defined by A_o, M_1, M_2, and M_3. A_1, A_2, and A_3 are part of the charged particle veto system. V_1 and the Veto House belong to the shower veto system.

Fig. 3 Schematic drawing of the photon detector. Gaps between the lead plates are filled with scintillator rods, with horizontal and vertical rods in successive gaps. Eight rods having the same x or y coordinate are connected optically to form one counter. There are 70 x- counters and 70 y- counters. These counters measure the x and y (transverse) projections of one or more photon showers in the detector.

Fig. 4 Spectrum of M^2 at 101 GeV/c for events satisfying cuts 1-5.

Fig. 5 (a-d): Distributions of $d\sigma/dt$ for reaction (1) at 20.7, 40.6, 66 and 101 GeV/c. The errors shown are statistical only.

Fig. 6 Distributions of $d\sigma/dt$ in the small t region for reaction (1) at 20.7, 40.6, 66 and 101 GeV/c. The errors shown are statistical only. Horizontal error bars indicate values of Δt, the experimental t resolution, at 101 GeV/c.

Fig. 7 A plot of the integrated cross section σ_{CEX} as a function of p_{lab}. The solid curve is a fit to the data of Ref. [3] and of the present experiment.

Fig. 8 Plots of $d\sigma/dt$ for reaction (1) versus p_{lab} for a number of different t values. The solid curves give the results of a fit to expression (4), using the data of Ref. [3] and of the present experiment.

Fig. 9 Effective trajectory values for reaction (1).

Fig. 10 The difference $\Delta\sigma$ of the $\pi^- p$ and $\pi^+ p$ total cross sections, plotted as a function of p_{lab}. The solid and dashed curves are predictions for $\Delta\sigma$ from the data of the present experiment, as described in the text.

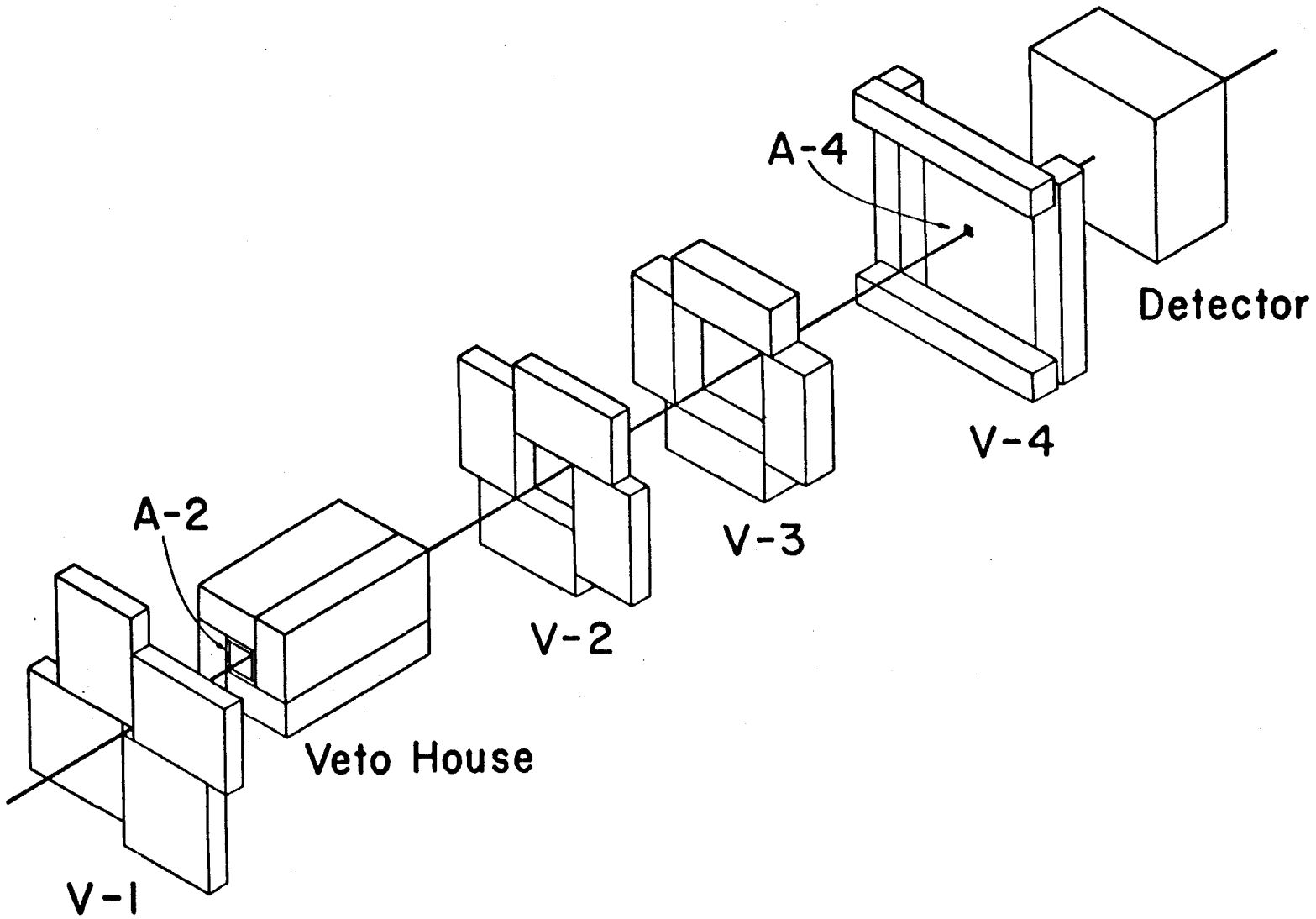

Figure 1

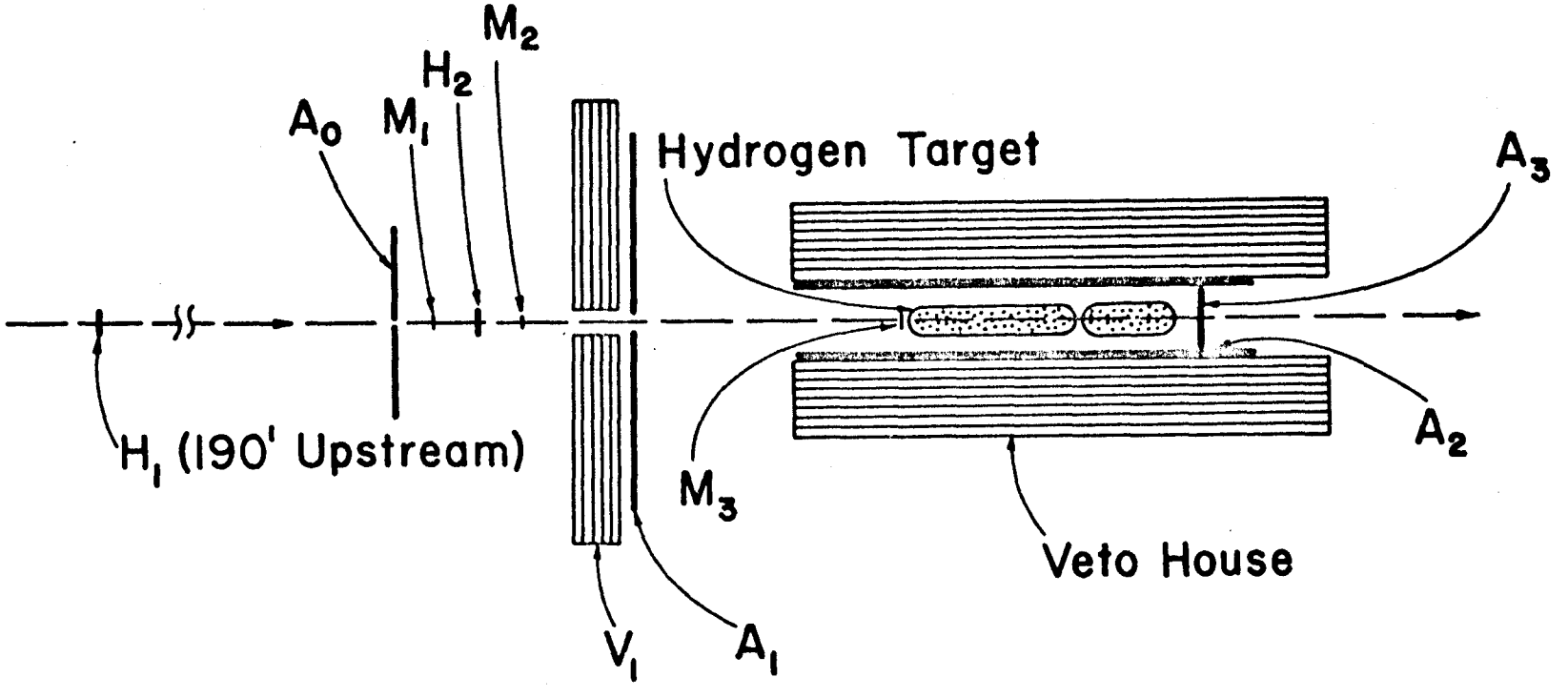
M2
H2
A0
M1
Hydrogen Target
A3
H1 (190' Upstream)
M3
A2
Veto House
V1
A1

Figure 2

Figure 3

PHOTON DETECTOR SCHEMATIC

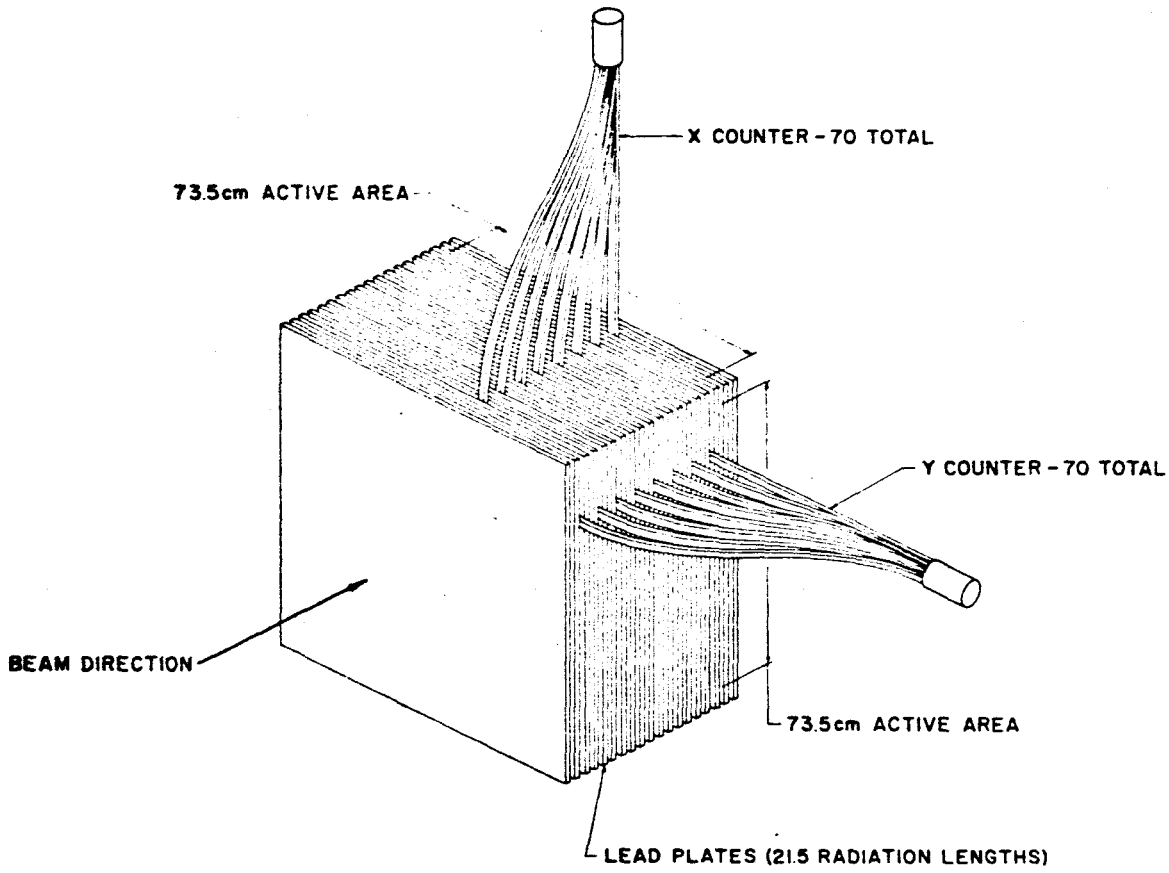

Figure 4

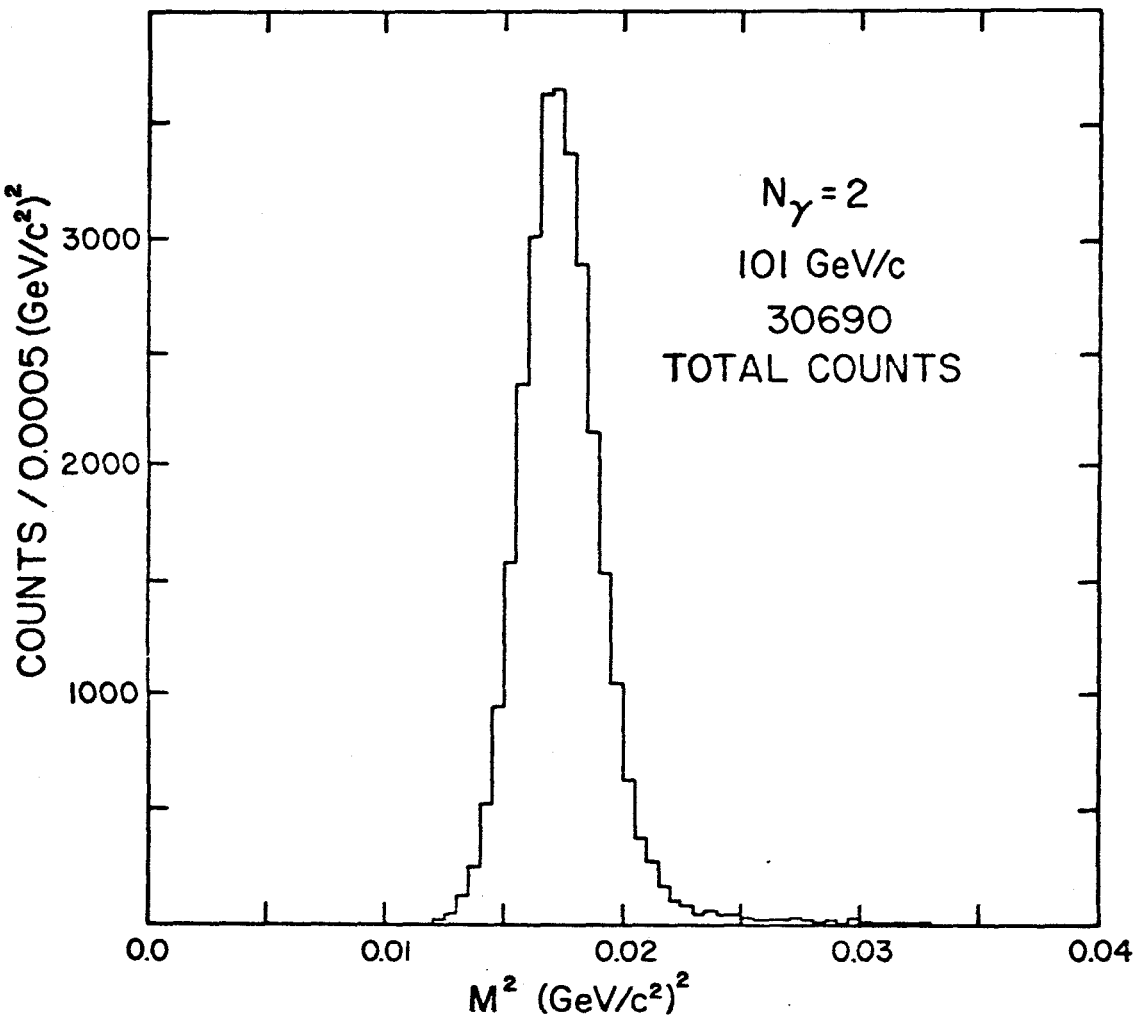
$N_\gamma = 2$
101 GeV/c
30690
TOTAL COUNTS
COUNTS / 0.0005 (GeV/c²)²
3000
2000
1000
0.0
0.01
0.02
0.03
0.04
M² (GeV/c²)²

Figure 5(a)

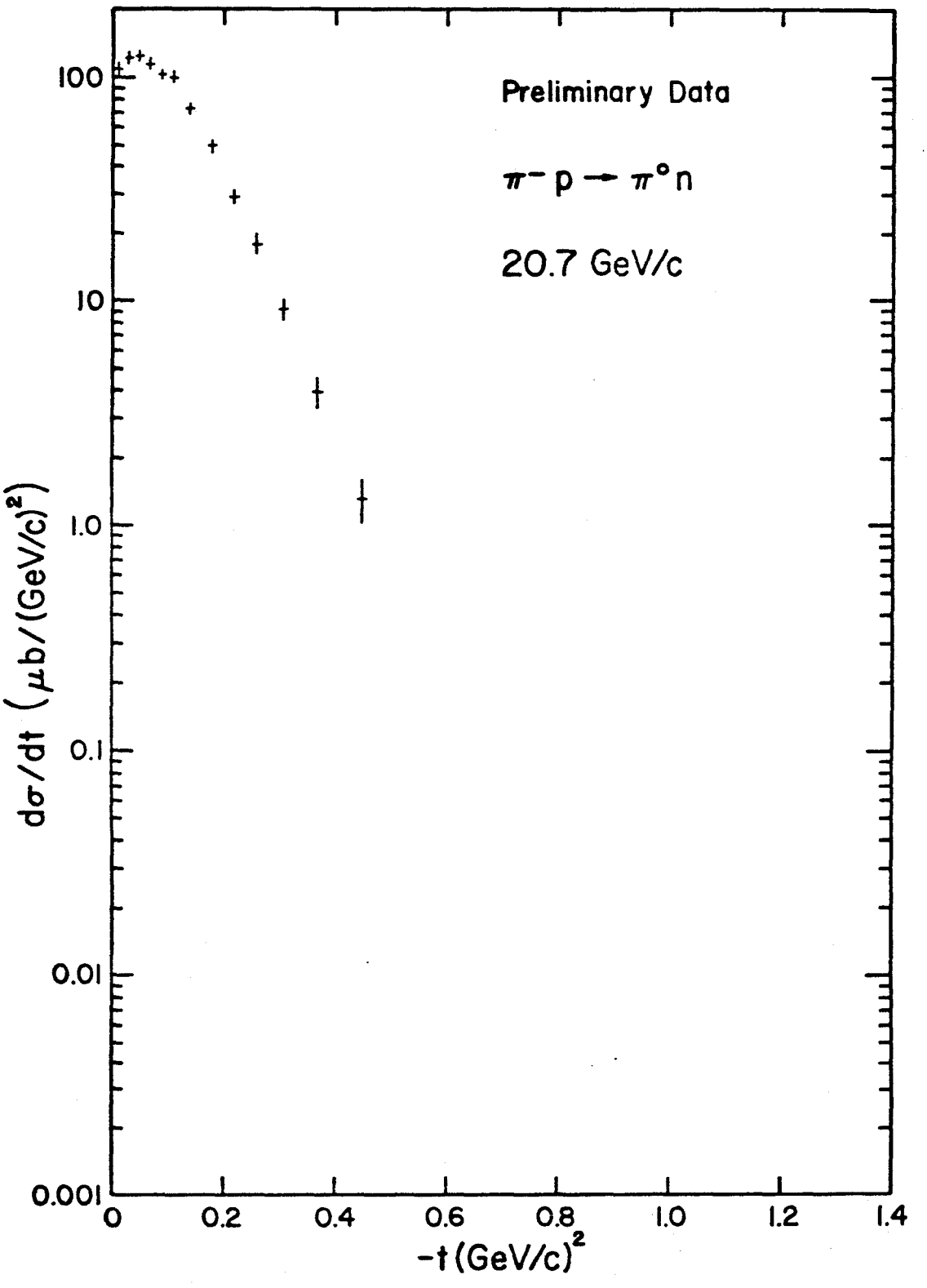
Preliminary Data
$\pi^- p \rightarrow \pi^\circ n$
20.7 GeV/c
100
10
1.0
0.1
0.01
0.001
$d\sigma/dt$ ($\mu b/(GeV/c)^2$)
0
0.2
0.4
0.6
0.8
1.0
1.2
1.4
$-t\,(GeV/c)^2$

Figure 5(b)

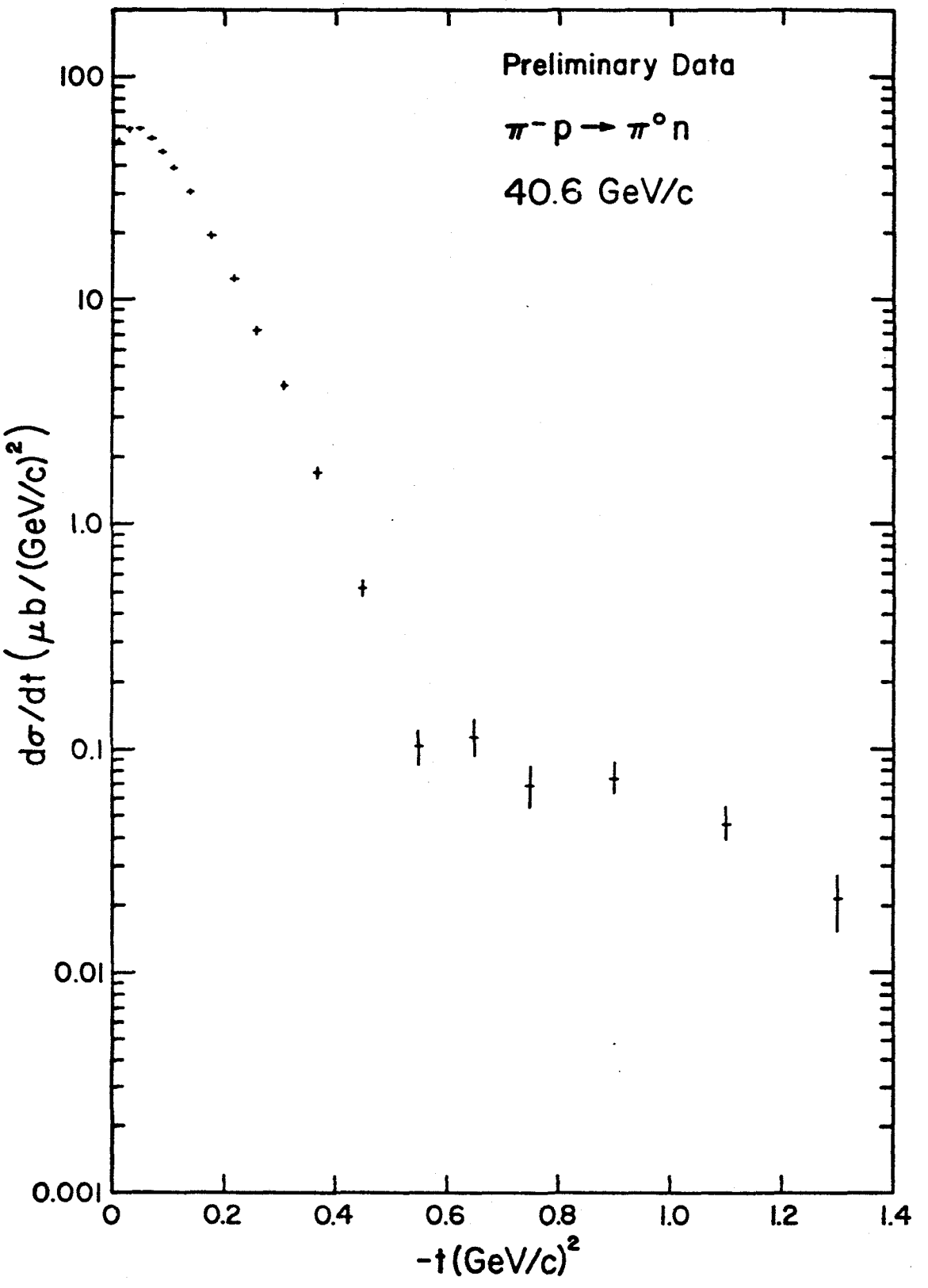
Preliminary Data
$\pi^- p \rightarrow \pi^0 n$
40.6 GeV/c
100
10
1.0
0.1
0.01
0.001
$d\sigma/dt\ (\mu b/(GeV/c)^2)$
0
0.2
0.4
0.6
0.8
1.0
1.2
1.4
$-t\ (GeV/c)^2$

Figure 5(c)

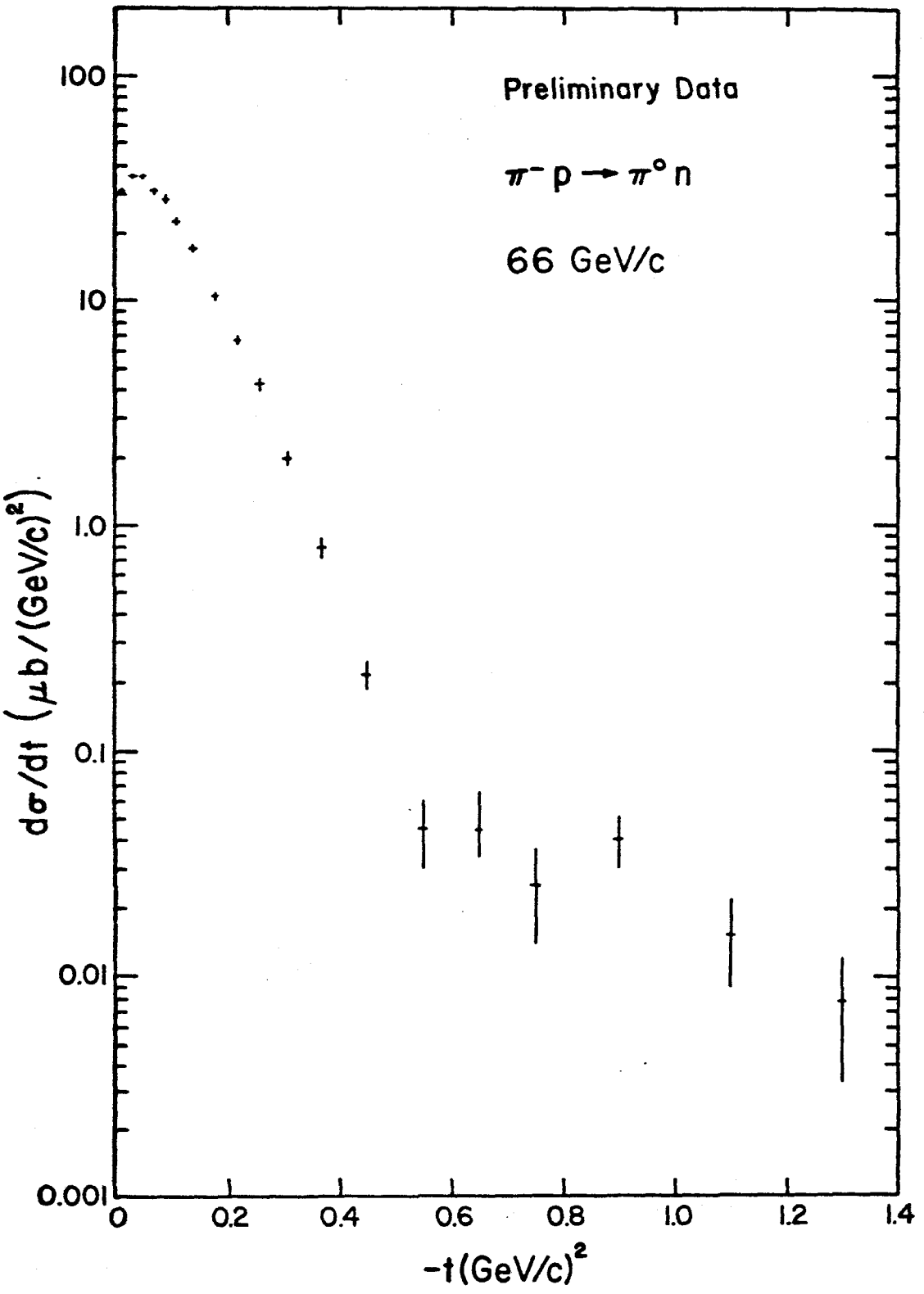
Preliminary Data
$\pi^- p \rightarrow \pi^0 n$
66 GeV/c
100
10
1.0
0.1
0.01
0.001
$d\sigma/dt$ ($\mu b/(GeV/c)^2$)
0
0.2
0.4
0.6
0.8
1.0
1.2
1.4
$-t(GeV/c)^2$

Figure 5(d)

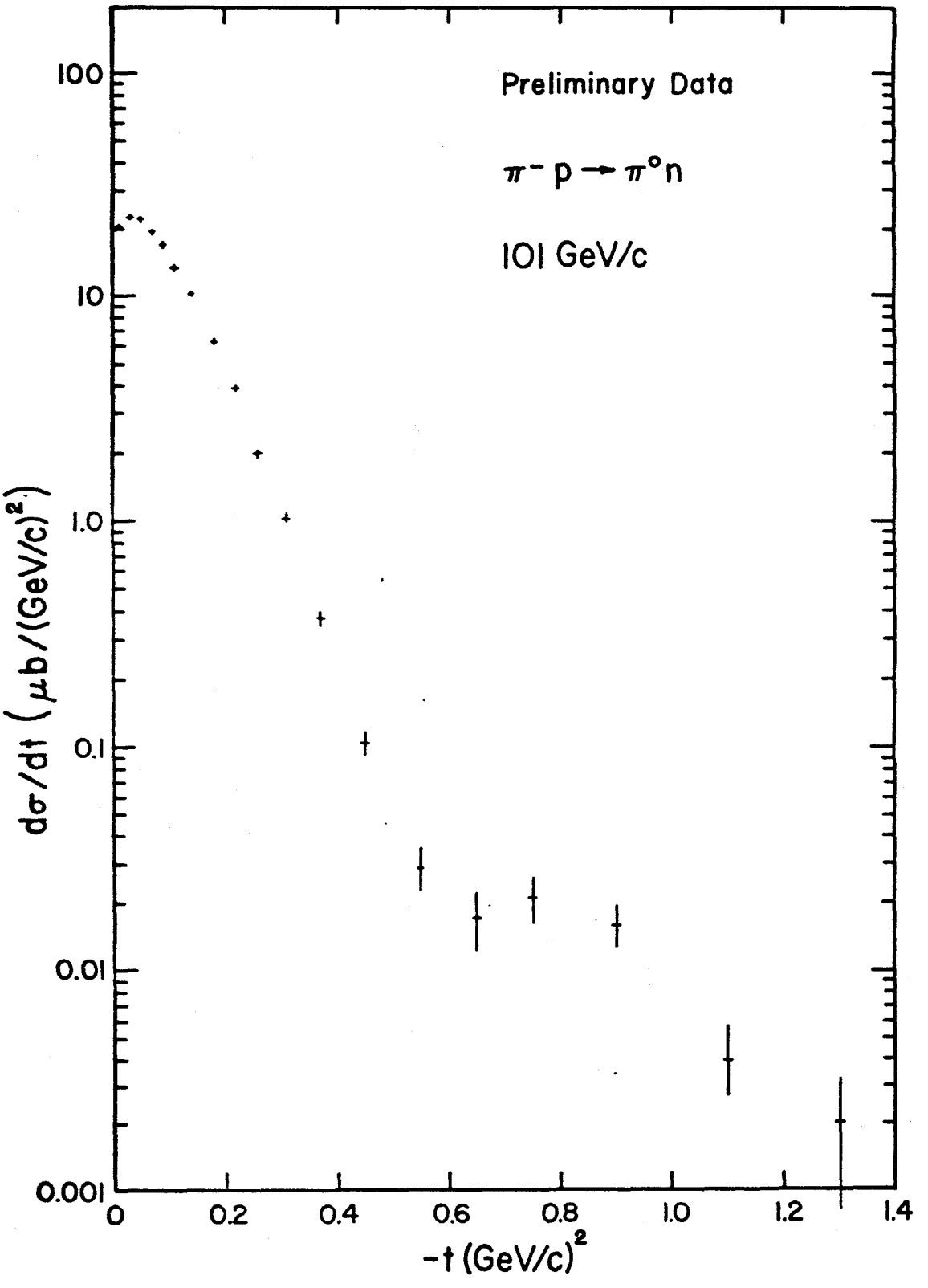
Preliminary Data
$\pi^- p \rightarrow \pi^0 n$
101 GeV/c
100
10
1.0
0.1
0.01
0.001
$d\sigma/dt$ ($\mu b/(GeV/c)^2$)
0
0.2
0.4
0.6
0.8
1.0
1.2
1.4
$-t$ $(GeV/c)^2$

Figure 6

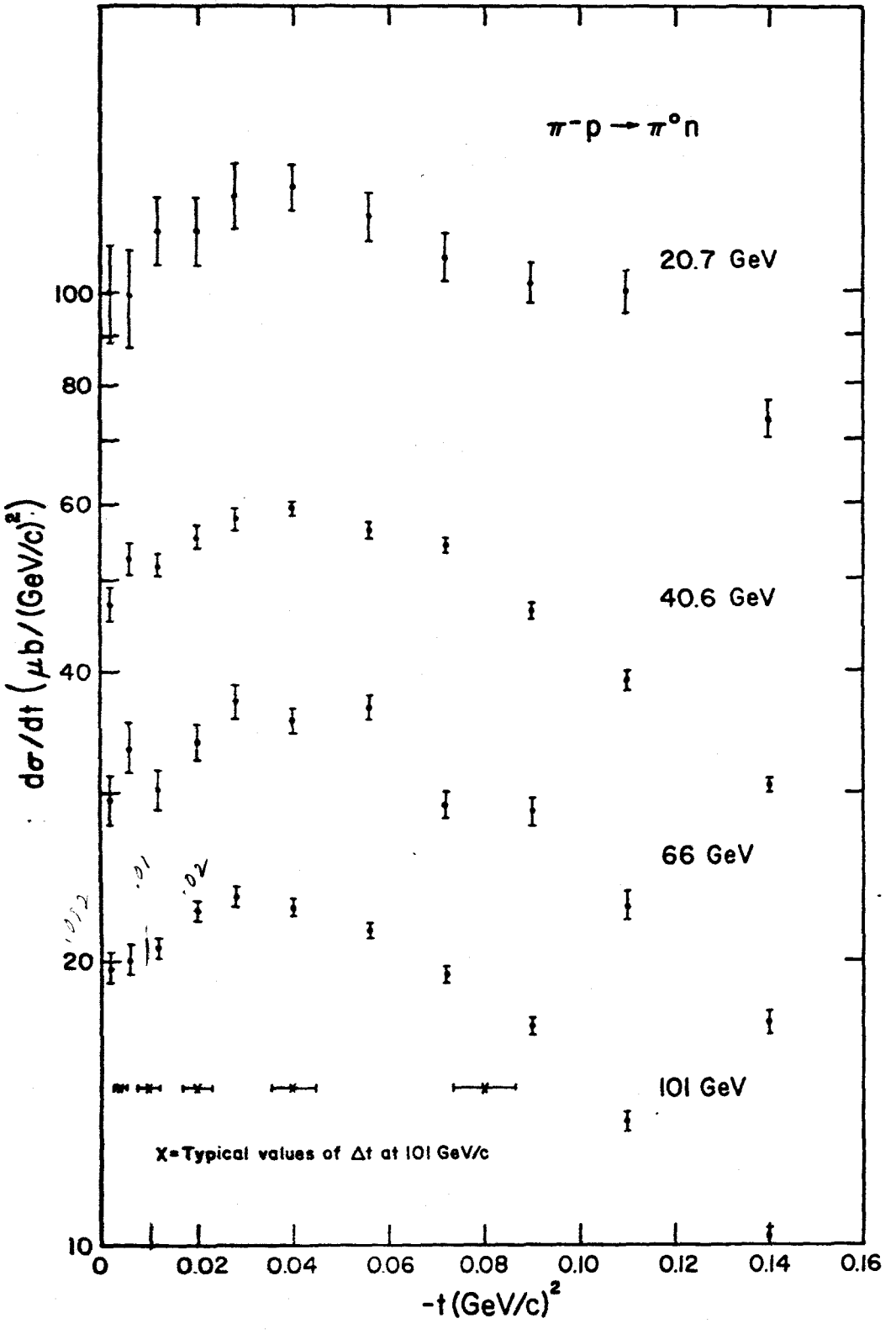
$\pi^- p \rightarrow \pi^0 n$
20.7 GeV
40.6 GeV
66 GeV
101 GeV
X=Typical values of Δt at 101 GeV/c
dσ/dt (μb/(GeV/c)²)
-t (GeV/c)²
100
80
60
40
20
10
0
0.02
0.04
0.06
0.08
0.10
0.12
0.14
0.16

Figure 7

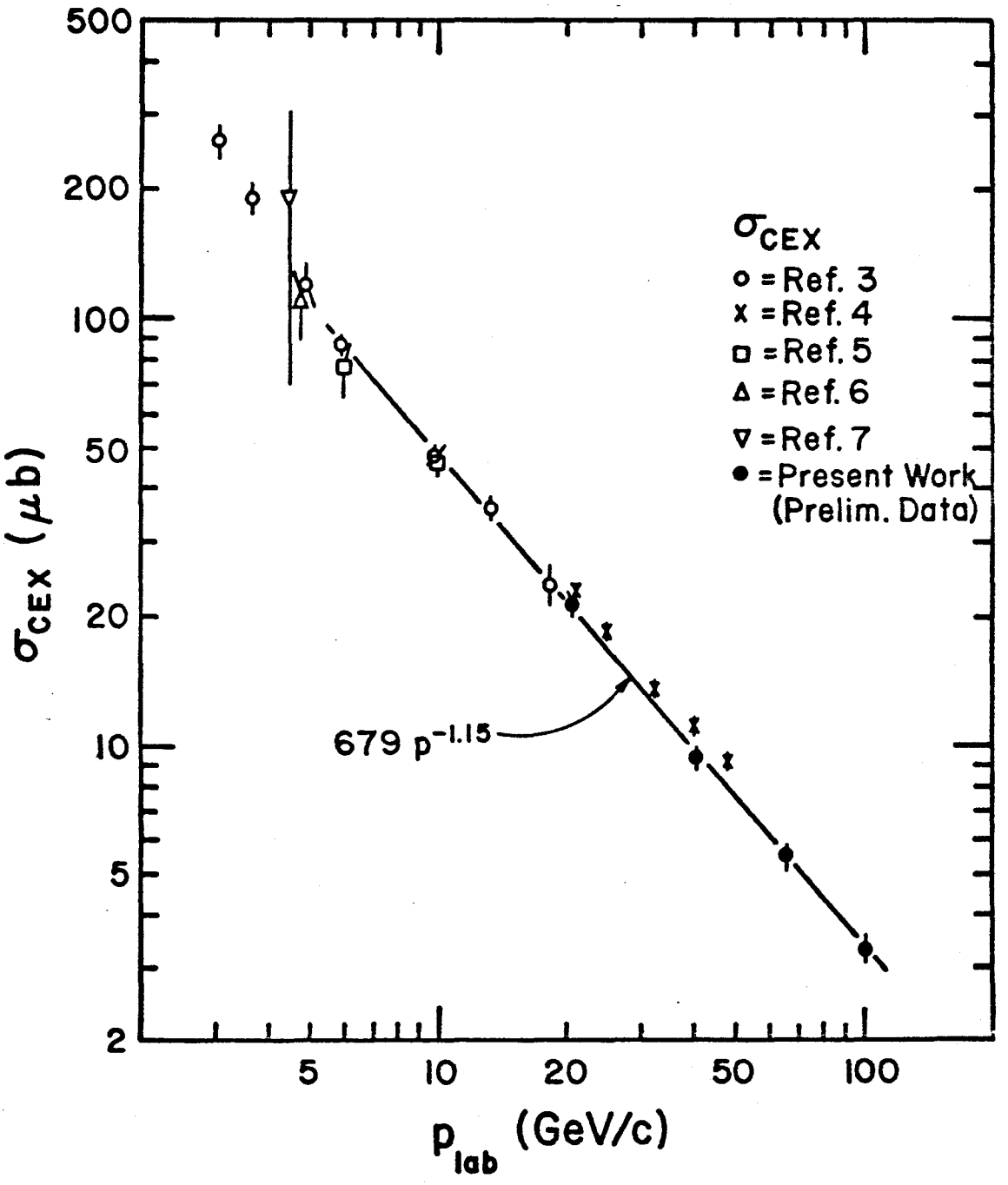
500
200
100
50
20
10
5
2
σ_{CEX} (μb)
5
10
20
50
100
p_{lab} (GeV/c)
σ_{CEX}
o = Ref. 3
x = Ref. 4
□ = Ref. 5
Δ = Ref. 6
∇ = Ref. 7
● = Present Work
(Prelim. Data)
679 $p^{-1.15}$

Figure 8

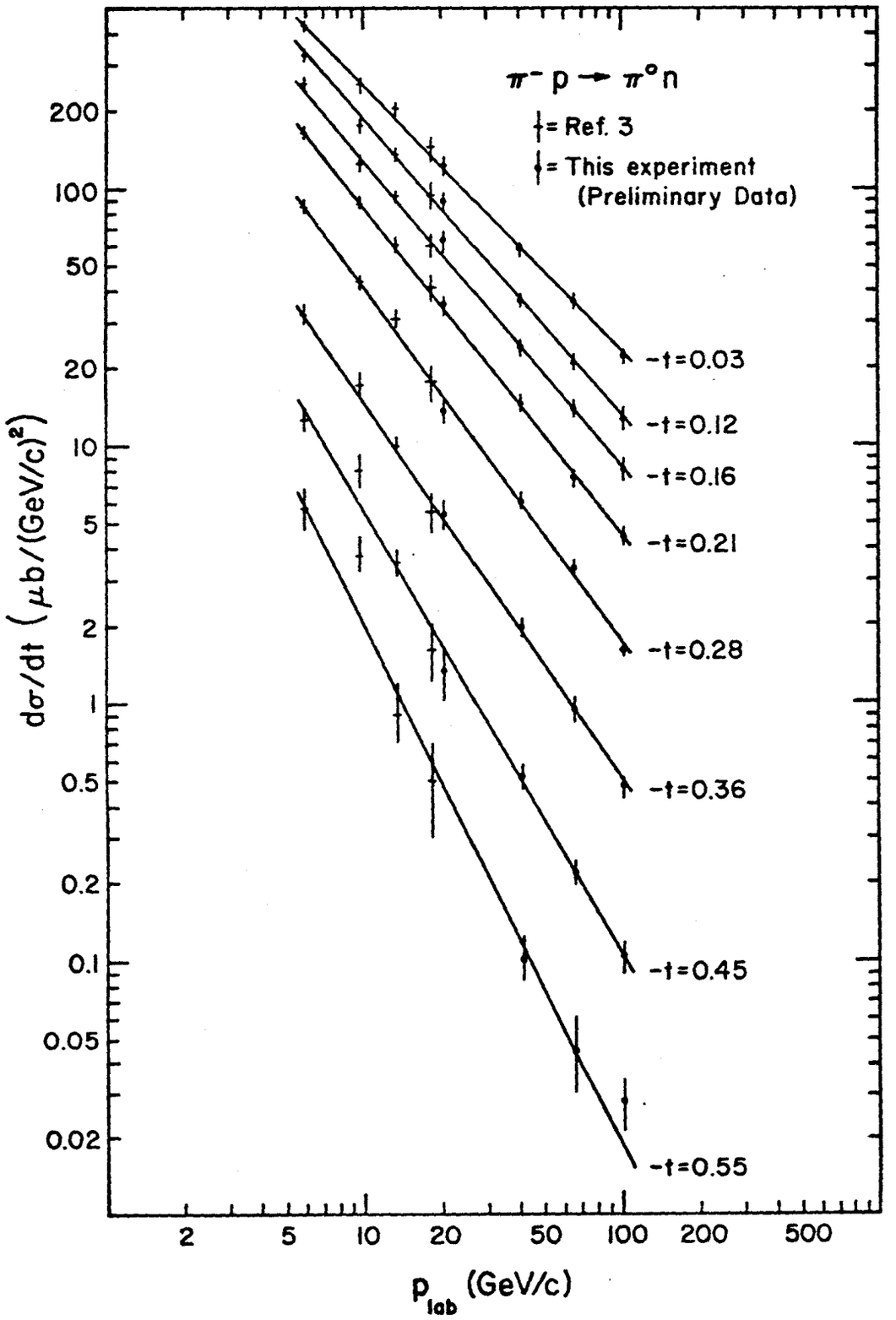
$\pi^- p \rightarrow \pi^0 n$
= Ref. 3
= This experiment (Preliminary Data)
-t=0.03
-t=0.12
-t=0.16
-t=0.21
-t=0.28
-t=0.36
-t=0.45
-t=0.55
$d\sigma/dt$ ($\mu b/(GeV/c)^2$)
200
100
50
20
10
5
2
1
0.5
0.2
0.1
0.05
0.02
2
5
10
20
50
100
200
500
p_{lab} (GeV/c)

Figure 9

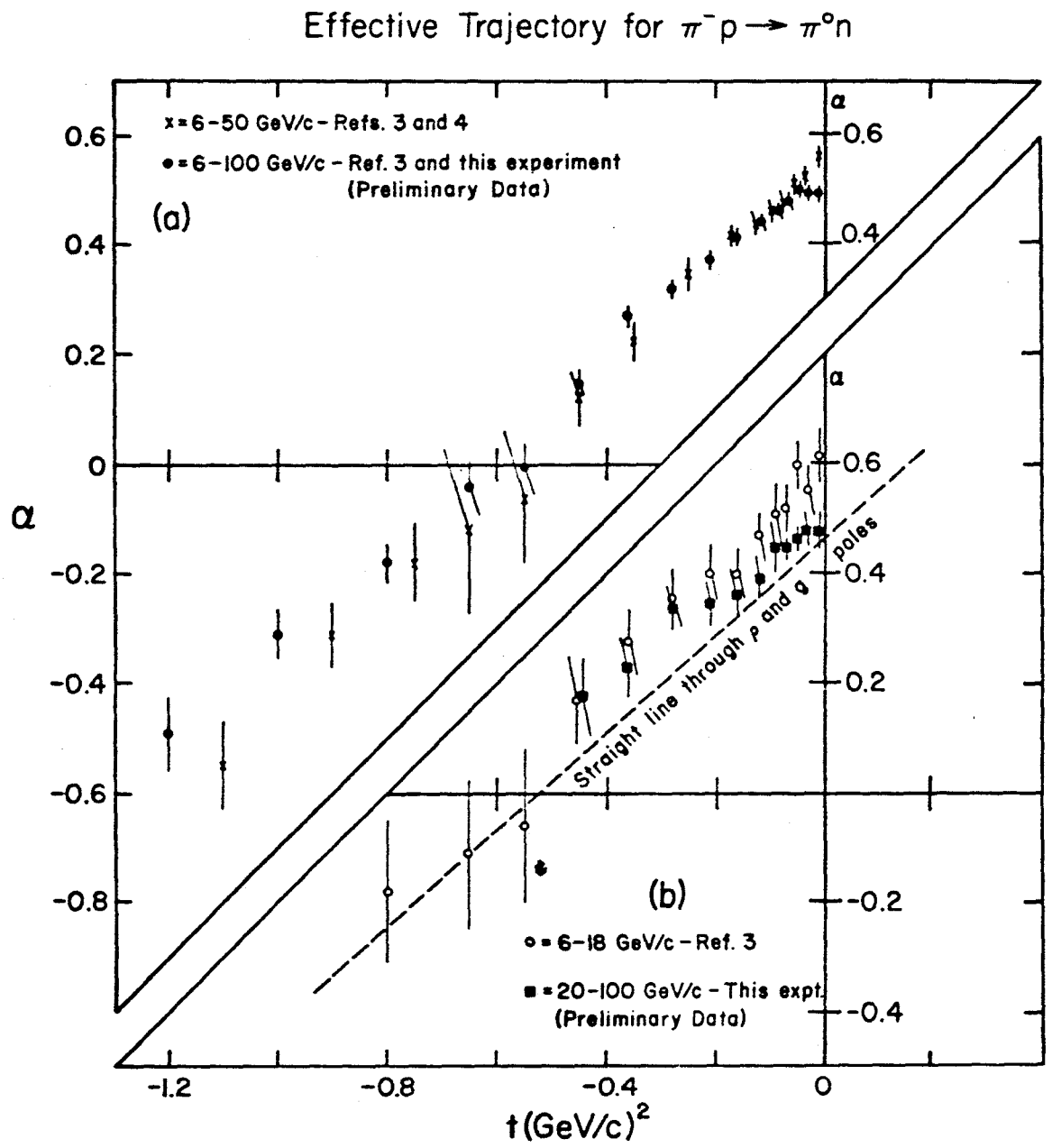
Effective Trajectory for $\pi^- p \rightarrow \pi^0 n$
x = 6-50 GeV/c - Refs. 3 and 4
• = 6-100 GeV/c - Ref. 3 and this experiment
(Preliminary Data)
(a)
(b)
Straight line through ρ and g poles
○ = 6-18 GeV/c - Ref. 3
■ = 20-100 GeV/c - This expt.
(Preliminary Data)
α
t (GeV/c)^2
0.6
0.4
0.2
0
-0.2
-0.4
-0.6
-0.8
-1.2
-0.8
-0.4
0

Figure 10

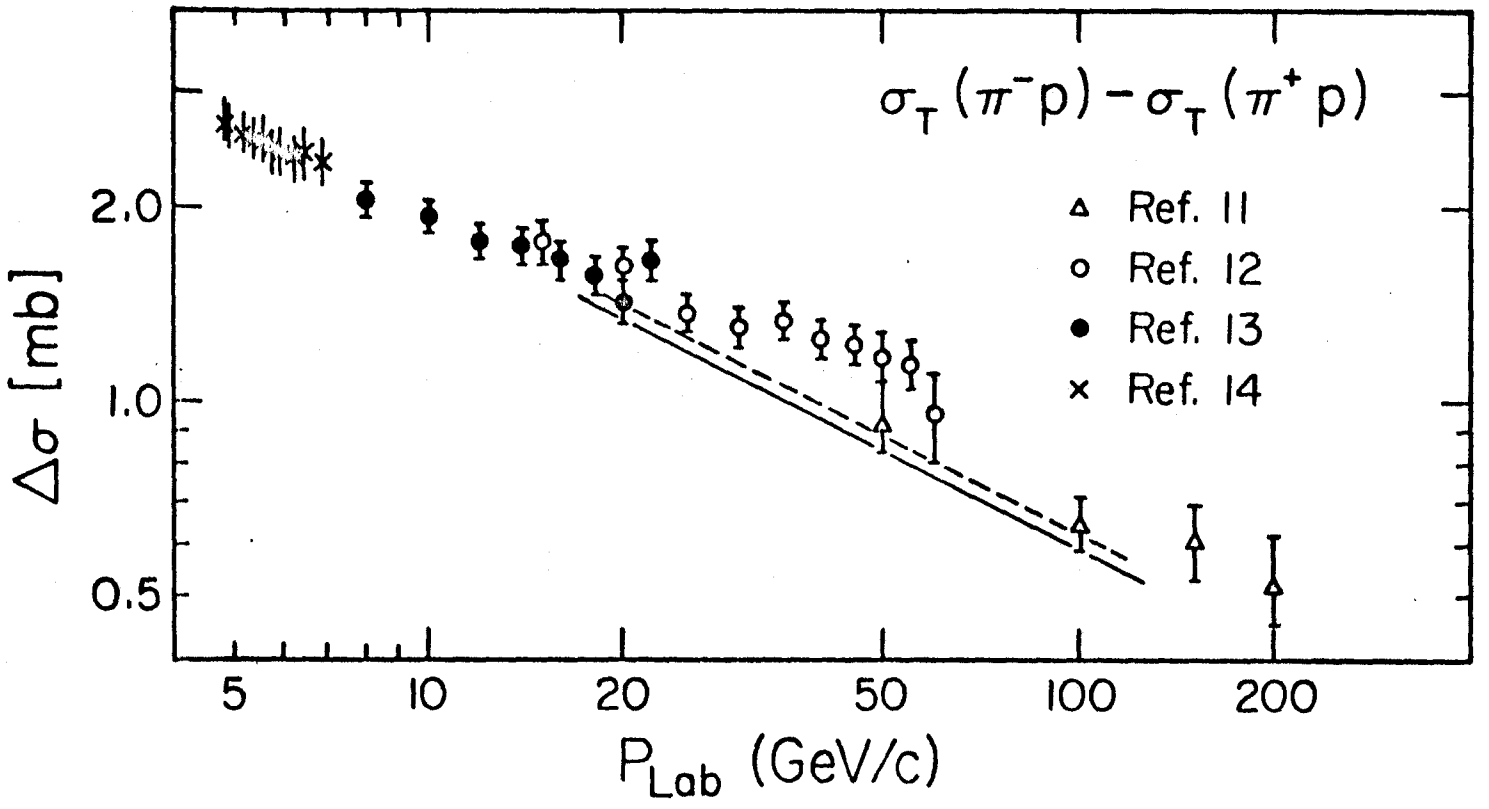
$\sigma_T(\pi^- p) - \sigma_T(\pi^+ p)$
Ref. 11
Ref. 12
Ref. 13
Ref. 14
$\Delta\sigma$ [mb]
2.0
1.0
0.5
5
10
20
50
100
200
P_{Lab} (GeV/c)